

DOI: 10.1002/adhm.((please add manuscript number))

Article type: Full Paper

# Boron-doped nanocrystalline diamond micro-electrode arrays monitor cardiac action potentials

Vanessa Maybeck<sup>1</sup>, Robert Edgington<sup>1</sup>, Alexandre Bongrain, Joseph O. Welch, Emanuel Scorsone, Philippe Bergonzo, Richard B. Jackman, and Andreas. Offenhäusser\*

((Optional Dedication))

Dr. Vanessa Maybeck, Prof. A. Offenhäusser ICS/PGI-8 Bioelectronics, Forschungszentrum Jülich GmbH Juelich, 52425 (Germany)
E-mail: ((a.offenhaeusser@fz-juelich.de))
Dr. R. Edgington, Mr. J. Welch, Prof. R.B. Jackman LNC, University College London
London, WC1H 0AH (United Kingdom)
Dr. E. Scorsone, Prof. P. Bergonzo
CEA LIST, Diamond Sensors Laboratory, CEA-Tech
Gif-sur-Yvette, F-91191 (France)

Keywords: ((nanocrystalline diamond, action potential, MEA))

## **Abstract**

The expansion of diamond based electronics in the area of biological interfacing has not been as thoroughly explored as applications in electrochemical sensing. However, the biocompatibility of diamond, large safe electrochemical window, stability, and tunable electronic properties provide opportunities to develop new devices for interfacing with electrogenic cells. We present the fabrication of micro electrode arrays (MEAs) with boron doped nanocrystalline diamond (BNCD) electrodes and their interfacing with cardiomyocyte-like HL-1 cells to detect cardiac action potentials. We show a non-reductive means of structuring doped and undoped diamond on the same substrate. The resulting BNCD electrodes show high stability under mechanical stress generated by the cells. It is shown that by fabricating the entire surface of the MEA with NCD, in patterns of conductive doped, and

<sup>&</sup>lt;sup>1</sup> These authors contributed equally.



isolating undoped regions, signal detection may be improved up to fourfold over BNCD electrodes passivated with traditional isolators.

## 1. Introduction

Diamond based electronics have become a topic of great interest over the last decade. Doped diamond materials of single-, micro- and nano-crystallinity have been used to design novel electronic devices. [1-6] The biocompatibility and electrochemical window of these materials make biological and biochemical applications particularly relevant. [2-4,7,8] Furthermore, by varying the doping, diamond can be tuned from 10<sup>-6</sup> S m<sup>-1</sup> (insulating) to 10<sup>4</sup> S m<sup>-1</sup> (metal-like conductive), making doped diamond a suitable material for electrode applications. Diamond was used as a macro electrode in 1987, [8] and in 2002 a diamond microelectrode array (MEA) was reported. [9] That work demonstrated that boron-doped diamond (BDD) electrode arrays with 25-30 µm diameter could be used for electrochemical analysis of ferrocyanide and ascorbic acid. A diamond passivated, diamond MEA was later designed and used for electrochemical measurement of (NH<sub>3</sub>)<sub>6</sub>RuCl<sub>3</sub>.<sup>[10]</sup> Subsequently, diamond MEA applications have focused on the detection of redox active compounds by cyclic voltammetry, [8,11] water treatment, and electro-synthesis. [12,13] Diamond based electrodes have been thoroughly developed for electrochemical sensing; however, the increase in diamond electrode use to detect bioelectric cell signals has not kept pace. It was not until 2006 that macro diamond electrodes recorded electrical signals from cells.<sup>[14,15]</sup> In 2008 a diamond electrode was implanted into a guinea pig's auditory cortex and successfully recorded extracellular neural signals in vivo. [16] However, the SNR in vivo appeared to be negatively affected by the low conductivity of diamond. [16,17] Since then, diamond microelectrodes have been increasingly tested for *in vivo* and *in vitro* use<sup>[18]</sup> and Bergonzo et al.<sup>[19]</sup> have shown that a flexible diamond/polyimide MEA induces minimal glial scarring after 14 weeks of implantation. However, the extensive use of diamond MEAs to interface with cells



electrically has not been realized. Many studies are presented for the suitability of diamond devices as implants, [20-23] but electrical recordings with single cell resolution remain rare. [24] Other forms of carbon, such as carbon nanotubes (CNTs) [25] have been used to detect cell signals with encouraging SNR, suggesting electrical impulse sensing using BNCD MEAs should be investigated.

#### 2. Results & Discussion

Four versions of BNCD electrode devices were fabricated and compared to Au MEAs with standard ONO passivation (see also the Experimental Section). The chips produced by our developed etching protocols and patterned growth system were evaluated in purely electrical systems, with artificially applied signals, and in the bioelectronic system of HL-1 culture. HL-1 cells were chosen because they provide high device coverage and predictable signal generation, though the performance with these cells will be indicative of whether the device can detect signals from other electrogenic cells as well.

When an externally generated sine signal was applied to the bath, BNCD electrodes demonstrated bandwidth ranges similar to planar metal electrodes (**Figure 1**). The maximum amplification achieved relative to the hardware's theoretical capability was 67±9%, 85±12%, 74±12% 29±17% and 59±26% for SU8 passivated BNCD with BNCD bondpads, SU8 passivated BNCD with TiSi<sub>2</sub> bondpads, ONO passivated BNCD, NCD passivated BNCD, and ONO passivated Au, respectively (N as in **Figure 1**). It was found to be necessary to connect the MEAs to metal via the TiSi<sub>2</sub> used for BNCD adhesion rather than via the BNCD directly. Although the BNCD is expected to display near metallic behaviour in its bulk at 10<sup>21</sup> cm<sup>-3</sup> doping, we measure its resistance as 30 Ohm m and the diamond likely supports a Schottky barrier at the Ag-diamond interface. The more reactive Ti-diamond interface overcomes this problem, likely by forming a carbide interface, leading to a more ohmic-like contact. The TiSi<sub>2</sub> film had a resistance of 1.4 x 10<sup>-6</sup> Ohm m. The bandwidth of all chips



lies within the range suitable for detecting cell APs (150-1100 Hz for the sodium and potassium components).

HL-1 cells were cultured for several days within glass ring culture chambers on top of the electrode arrays (see Figure 2 and the Experimental Section for details). The HL-1's spontaneous generation of action potential waves once a tissue forms make them an excellent cell type to test novel AP sensing devices. Cell signals were detected on multiple electrodes of all BNCD MEA designs, allowing characterisation of the AP propagation through the tissue (Figure 3) and providing insight into the coupling of the cell and the electrode (Figure 4). Because the AP wave moves across the tissue, arrival of each AP is shifted in time, providing additional evidence that the signals are APs. Propagation waves should appear as traveling lines or radiating rings (depending on the location of the pacemaker cell) when the time of an AP is plotted for each electrode channel. The propagation of APs on BNCD MEAs was 10-30 mm s<sup>-1</sup>, which is comparable to  $7 \pm 5$  mm s<sup>-1</sup> observed on gold electrodes passivated with SiO<sub>2</sub>/Si<sub>3</sub>N<sub>4</sub>/SiO<sub>2</sub> (ONO), and 7-28 mm s<sup>-1</sup> reported previously. [30, 31] This is a further indicator that the cells are healthy and performing normally on the diamond substrates (Figure 3). Variability among channels is expected because cells can exhibit different AP shapes as determined by the mixture of proteins expressed. Furthermore, the coupling of the cell to the electrode (electrode coverage, cleft height, and seal resistance) influences signal shape. On a functional device, one expects the subsequent APs fired by one cell over a specific electrode to be similar. This was found for BNCD electrodes with similar variability to equivalent metal electrodes (Figure 4). High variability from spike to spike on an electrode would suggest that the recording is from an ensemble rather than a single spiking unit. Furthermore, the shape of the APs detected shows that BNCD electrodes often detect a sharp pre-peak before the AP (Figure 4), a form associated with high seal resistance between the cell and electrode according to mathematical models.<sup>[32]</sup>



ONO passivation was more stable than SU8. However, in rare cases, defects in the ONO layer exhibited double spike detection, presumably through pinholes or cracks (Figure 5). Which spike of the pair was detected by the fabricated electrode could be determined by calculating the propagation direction from channels that registered only one AP per heartbeat. In some cases, the coupling to the defect led to even higher SNRs than the signal recorded from the electrode. This suggests that optimisation of electrode size and structure could lead to further improvements in BNCD MEA performance. Though ONO and NCD are both more stable than SU8, the advantages of NCD make it a preferable passivation. NCD induces less inflammation and acute biological response to implants than Si technology [33]. NCD films are also consistently sealed at thinner film thickness than ONO (<400 nm vs. >1.5 μm, respectively, see also the Supporting Information). Ideal chips should therefore present a purely diamond surface for improved cell-device coupling. In contrast to lapidary methods of fabricating doped/undoped diamond structures, [10] the method developed here, using Cr cap masking, allows non-reductive deposition of patterned diamond layers on top of existing diamond layers. Briefly, since diamond films are grown from seed diamond slurry affixed to a surface, by selectively blocking areas of the seeds, growth of a film can be locally inhibited, (Figure 2). It also lacks the topography requirements of the lapidary method. Furthermore, our method avoids the complicated etching though intrinsic diamond to doped diamond described previously, [17] alleviating stringent

from seed diamond slurry affixed to a surface, by selectively blocking areas of the seeds, growth of a film can be locally inhibited, (**Figure 2**). It also lacks the topography requirements of the lapidary method. Furthermore, our method avoids the complicated etching though intrinsic diamond to doped diamond described previously, [17] alleviating stringent controls on reactive ion etching (RIE). Removal of the seed diamonds under the Cr caps causes thinning of the passivation layer, but the shallow endpoint of this etch does not endanger the quality of the electrodes or passivation. Furthermore, despite the reduction in passivation to 330 nm, the diamond passivated chips did not exhibit excessive pinhole defects, typical of ONO or SU8 at this thickness. Diamond passivation of raised diamond feedlines was also more consistent than traditional passivations such as Si<sub>3</sub>N<sub>4</sub>, which often exhibit



defects where the passivation layer encounters sudden changes in substrate height (see also Supplementary Information).

BNCD electrodes survived the mechanical stresses of contractile cells without the defects commonly observed in other nanostructured materials after cell culture (loss of platinum black, removal of CNTs, [34] tipping of pillars, D. Brüggemann unpublished results). We conclude that the diamond layer remained on the surface during cell contraction by the lack of thinning-induced defects after multiple cultures and the contractile tension generated in mature HL-1 cells (cells did not pull themselves off of the surface). The diamond MEA's physical robustness makes it a durable and easy to handle device for repeated or long-term use. The surface structure of the all-diamond chips generated by the final plasma treatment is proposed to improve cell recordings in two ways. Firstly, the cells can better adhere to the topography of the surface, as has been shown previously for adhesion on rough materials. [25,33] Secondly, the increased surface area of the electrode lowers the impedance, allowing better AP detection. The SNR on unstructured diamond suggest that diamond optimisation can make all-diamond MEAs competitive with state of the art metal MEAs. Three dimensional structuring could also further improve diamond MEA performance, as shown for intentionally micro and nanostructured devices. [35-38]

The reduced passivation height, with maintained electrical isolation, further improves AP detection by reducing the cleft size between the cell and the device. The voltage change over the electrode is dependent on the change in distribution as well as the change in concentration of ions in the cleft due to cell activity. The coupling to the electrode is then improved by sealing the cell tightly to the passivation (adhesion to the rough surface), and by bringing the cell as close to the electrode as possible (a thinner passivation layer). The diamond's biocompatibility and structure improves adhesion and thus increases the seal resistance around the electrode preventing signal dissipation to the bath. Furthermore, the lower cleft



height achieved in NCD passivated MEAs improves capacitive coupling. A doubling of spike amplitude and up to a factor of four higher SNR was observed in some NCD passivated BNCD MEAs. Further refinement of the diamond-diamond fabrication technique may improve consistency and probe the limits of thinning the NCD passivation without introducing pinholes.

### 3. Conclusion

We fabricated several BNCD MEA designs with 64 microelectrodes, including MEAs with only diamond surfaces presented to the cells. The MEAs were tested as an electrical interface with the cardiomyocyte-like cell line HL-1.<sup>[26]</sup> HL-1 cells form an electrical syncytium and spontaneously generate APs that induce contraction. Thus, the diamond MEAs' ability to detect APs, map their progression through the tissue, and resist the mechanical and environmental assaults of interfacing with contractile tissue was shown.

The BNCD MEAs were characterized in both electrical and biological setups. The use of BNCD electrodes was shown to be promising for recording electrical signals from biological samples in addition to their established role in electrochemistry. We show that on average, BNCD electrodes can detect cardiac APs as well as gold electrodes. Furthermore, our proof-of-concept experiments show that all-diamond MEAs can perform up to a factor of fourfold better than planar metal electrodes of the same diameter. Improvement in the consistency of production would therefore raise diamond MEA performance above that of conventional materials

#### 4. Experimental Section

140 nm TiSi<sub>2</sub> was deposited by thermally annealing Ti and n-type polysilicon on oxidized Si wafers. The opaque Si wafer is necessary to withstand the growth temperatures of the diamond. TiSi<sub>2</sub> acts as an adhesion layer for the seed NDs and BNCD growth. 350 nm of highly boron doped (ca. 10<sup>21</sup> cm<sup>-3</sup>) BNCD was deposited by microwave plasma enhanced



chemical vapour deposition (MWPECVD) as described elsewhere. [39] An optimized RIE process for patterning diamond allowed the fabrication of BNCD electrode MEAs with single cell resolution. At first, traditional passivation materials were used to isolate the BNCD electrodes, such as 1500 nm thick SU8 epoxy or ONO of 500 nm each. NCD without intentional doping was developed as a passivation material for all-diamond chips. The challenge of NCD passivated chips is to achieve open BNCD electrodes within the NCD passivation, since precisely etching diamond on diamond is not established.

Diamond's stability complicates etching and processes are not as standardized as for traditional metals or semiconductors. In this work, an Inductively-Coupled Plasma Reactive Ion Etching (ICP RIE) process was developed for high aspect ratio patterning of diamond with smooth etched surfaces. High quality definition of features and biocompatibility was of higher priority than high etch rate on the thin MEA substrates. The process utilizes the selective chemical etching of reactive O2 to produce volatile CO and CO2, coupled with physical etching by argon bombardment to improve anisotropic etching. A 5:35 O2:Ar mixture offered higher aspect ratios and less pitting of the surface than mixtures where O2

exceeded Ar. Furthermore, a high platen power (PP: 200 W) was used to increase vertical

anisotropic etching. The development of this process builds on the key results found by

Hwang [40], Choi [41], Uetsuka [42] and Lee [43], see **Table 1**.

BNCD was etched in excess to expose the underlying TiSi<sub>2</sub> layer, as confirmed optically and by a change in the DC bias of the plasma. TiSi<sub>2</sub> removal between electrodes and feedlines was also confirmed optically. The BNCD pattern connected 64 electrodes (**Figure 2(b)**iii.b), with 20 µm diameter, to peripheral bond pads (**Figure 2(b)**iii.a) for connecting the chip to a carrier after passivation. The feedlines consisted of the BNCD and underlying TiSi<sub>2</sub>.

The opening of the passivation determines the electrode dimensions, and for SU8 and ONO the electrode was at the bottom of a 20  $\mu$ m diameter opening with a cleft depth of 1.5  $\mu$ m.



NCD passivation introduced additional complications due to the lack of etch selectivity between NCD and BNCD. Therefore, chrome capping of the electrodes and bondpads was used to selectively grow an undoped passivation layer of NCD using MWPECVD with the electrode opening already patterned (**Figure 2(b)**vi.a). To accomplish this, the surface was coated with nanodiamond seeds and fixed with a short MWPECVD process (**Figure 2(a)**: step iv), Cr caps were deposited on bondpads and electrodes using lift-off photolithography (**Figure 2(a)**: step v), undoped NCD was then grown on the remaining exposed seeds using MWPECVD (**Figure 2(a)**: step vi), after which Cr caps were removed with Cr etchant. A short RIE step removed ND seeds and ingrained Cr deposits (**Figure 2(a)**: step vii). Whilst some Cr could be remnant on the electrodes, this method obviates the diamond etch step that could damage BNCD electrodes if NCD growth was uneven.

Silver paste contacted the bondpads of passivated chips to the gold contacts of a PCB carrier. Glass rings were mounted on the chip and carrier to form a culture area and the PCB within the culture space was sealed with polydimethylsiloxane (PDMS) (**Figure 2(c)**). Finished BNCD MEAs were cultured with HL-1 cells <sup>[26]</sup> as a convenient model to validate BNCD MEAs in comparison to standard metal MEAs. HL-1 cells are maintained as stocks on tissue culture plastic flasks. When mature, beating cultures are dissociated and plated onto MEAs. Cells were grown in Claycomb's media supplemented with 0.1 mM epinephrine, 2 mM L-glutamine, 100 U ml<sup>-1</sup>: 100 μg ml<sup>-1</sup> penicillin/streptomycin, and 10% fetal bovine serum. Chips were measured at day *in vitro* (DIV) 3-5 when cells had formed a confluent layer and become active. HL-1 cells do not survive for long periods without splitting on any culture substrate due to crowding. Using primary neurons, cells were cultured on diamond MEAs for 10 days (data now shown).

Cells were removed from chips by digestion for at least 15 min in trypsin EDTA at 37°C.

After the first culture, chips were electrically characterized by applying a variable frequency



sine wave over the bath electrode, and returning a single channel at a time from the MEA amplifier output to the lock-in amplifier (Stanford Research, SR 830). This measured the actual amplification achieved at each frequency.

Spike analysis was performed using MatLab program M64 (Sommerhage), Origin 8 (OriginLab Corp.), and Med64 Conductor (Panasonic).

# Acknowledgements

We thank S. Ingebrandt for input on the early chip design, M. Jansen for TiSi<sub>2</sub> deposition and SU8 passivation, M. Banzet for wafer cutting and E. Neumann for SEM and FIB support. Thank you to B. Wolfrum for helpful discussion of the manuscript. This work was undertaken as part of the Sixth European Framework (FP6-NMP-2006-676033345) program DReAMS. VM acknowledges financial support by the International Helmholtz Research School on Biophysics and Soft Matter (BioSoft). RBJ acknowledges funding from the UK's Engineering and Physical Sciences Research Council (EPSRC, EP/F026110/1), whilst RE and JW are grateful for EPSRC-funded DTA PhD scholarships.

Received: ((will be filled in by the editorial staff))
Revised: ((will be filled in by the editorial staff))
Published online: ((will be filled in by the editorial staff))

- [1] H. Kawarada, Y. Araki, T. Sakai, T. Ogawa, and H. Umezawa, *Phys. Status Solidi A* **2001**, *185*, 79.
- [2] B. Rezek, D. Shin, H. Watanabe, and C.E. Nebel, Sens. Actuators B 2007, 122, 596.
- [3] R. Edgington, A.R. Ruslinda, S. Sato, Y. Ishiyama, K. Tsuge, T. Ono, H. Kawarada, and R.B. Jackman, *Biosens. Bioelectron.* **2012**, *33*, 152.
- [4] M. Dankerl, S. Eick, B. Hofmann, M. Hauf, S. Ingebrandt, A. Offenhaeusser, M. Stutzmann, and J.A. Garrido, *Adv. Funct. Mater.* **2009**, *19*, 2915.

- [5] A. Denisenko, G. Jamornmarn, H. El-Hajj, and E. Kohn, *Diamond Relat. Mater.* **2007**, *16*, 905.
- [6] H. El-Hajj, A. Denisenko, A. Bergmaier, G. Dollinger, M. Kubovic, and E. Kohn, *Diamond Relat. Mater.* **2008**, *17*, 409.
- [7] C.E. Nebel, B. Rezek, D. Shin, and H. Watanabe, *Phys. Status Solidi A* **2006**, *203*, 3273.
- [8] Y. Pleskov, Russ. J. Electrochem. 2002, 38, 1275.
- [9] K. Tsunozaki, Y. Einaga, T. Rao, and A. Fujishima, Chem. Lett. 2002, 5, 502.
- [10] M. Pagels, C.E. Hall, N.S. Lawrence, A. Meredith, T.G.J. Jones, H.P. Godfried, C.S.J. Pickles, J. Wilman, C.E. Banks, R.G. Compton, and L. Jiang, *Anal. Chem.* **2005**, *77*, 3705.
- [11] M. Hupert, A. Muck, R. Wang, J. Stotter, Z. Cvackova, S. Haymond, Y. Show, and G. Swain, *Diamond Relat. Mater.* **2003**, *12*, 1940.
- [12] M. Panizza and G. Cerisola, *Electrochim. Acta* **2005**, *51*, 191.
- [13] A. Kraft, Int. J. Electrochem. Sci. 2007, 2, 355.
- [14] J. Halpern, S. Xie, G. Sutton, B. Higashikubo, C. Chestek, H. Lu, H. Chiel, and H. Martin, in *Diamond Relat. Mater.* **2006**, *15*, 4-8.
- [15] J. Park, V. Quaiserova-Mocko, K. Peckova, J.J. Galligan, G.D. Fink, and G.M. Swain, *Diamond Relat. Mater.* **2006**, pp. 761–772.
- [16] M.W. Varney, D.M. Aslam, A. Janoudi, H.-Y. Chan, and D.H. Wang, *Biosensors***2011**, *I*, 118.
- [17] M.W. Varney, Z. Cao, and D.M. Aslam, *NEMS*, **2010**, pp. 1116–1119.
- [18] J. Park, V. Quaiserova-Mocko, B. A. Patel, M. Novotny, A. Liu, X. Bian, J. J. Galligan, and G. M. Swain, *Analyst* **2008**, *133*, 17.

- [19] P. Bergonzo, A. Bongrain, E. Scorsone, A. Bendali, L. Rousseau, G. Lissorgues, P. Mailley, Y. Li, T. Kauffmann, F. Goy, B. Yvert, J.A. Sahel, and S. Picaud, *IRBM* **2011**, *32*, 91.
- [20] M. Bonnauron, S. Saada, L. Rousseau, G. Lissorgues, C. Mer, and P. Bergonzo, *Diamond Relat. Mater.* **2008**, *17*, 1399.
- [21] Z. Gao, V. Carabelli, E. Carbone, E. Colombo, M. Dipalo, C. Manfredotti, A. Pasquarelli, M. Feneberg, K. Thonke, E. Vittone, and E. Kohn, Journal of *Micro-Nano Mechatronics* **2011**, *6*, 33.
- [22] K. Ganesan, A. Stacey, H. Meffin, S. Lichter, U. Greferath, E.L. Fletcher, and S. Prawer, in *EMBC'10* **2010**, pp. 6757–6760.
- [23] L. Tang, J. Exp. Med. 1993, 178, 2147.
- [24] A. Bongrain, A. Bendali, G. Lissorgues, L. Rousseau, B. Yvert, E. Scorsone, P. Bergonzo, and S. Picaud, in *CORD Conference Proceedings* **2011**, pp. 378.
- [25] A. Shoval, C. Adams, M. David-Pur, M. Shein, Y. Hanein, and E. Sernagor, *Front. Neuroeng.* **2009**, *2*, 4.
- [26] W. C. Claycomb, N. Lanson, B. Stallworth, D. B. Egeland, J. B. Delcarpio, A. Bahinski, and N. J. Izzo, *PNAS*, **1998**, *95*, 2979.
- [27] T. Borst and O Weis, *Phys. Status Solidi C* **1996**, *154*(1), 423–444.
- [28] M. Gaowei, E.M. Muller, A.K. Rumaiz, C. Weiland, E. Cockayne, J. Jordan-Sweet, J. Smedley, and J.C. Woicik, *Appl. Phys. Lett.* **2012**, *100*, 201606.
- [29] H.J. Looi, L.Y.S. Pang, M.D. Whitfield, J.S. Foord, and R.B. Jackman, *Diamond Relat. Mater.* **2000**, *9*, 975–981.
- [30] S. Eick, in *Extracellular Stimulation of Individual Electrogenic Cells with Micro-Scaled Electrodes* **2010** RWTH Aachen, Germany, pp. 142-145.

- [31] L. Hess, M. Jansen, V. Maybeck, M. v Hauf, M. Siefert, M. Stutzmann, I. D. Sharp, A. Offenhaeusser, and J. A. Garrido, *Adv. Mater.*, **2011**, *23*, 5045.
- [32] M. Schottdorf, B. Hofmann, E. Kaetelhoen, A. Offenhaeusser, B. Wolfrum, *Phys. Rev. E* **2012**, *85*, 031917.
- [33] P.Bajaj, D. Akin, A. Gupta, D. Sherman, B. Shi, O. Auciello, R. Bashir, *Biomed. Microdevices* **2007**, *9*, 787.
- [34] Y. Hanein. *How Many Neurons Does It Take to Change a Lightbulb?* Talk. IBN-2, Forschungszentrum Juelich GmbH, Juelich, Germany (6 Apr **2011**).
- [35] D. Brueggemann, B. Wolfrum, V. Maybeck, Y. Mourzina, M. Jansen, A. Offenhaeusser, *Nanotechnology*, **2011**, *22*, 265104.
- [36] S.A. Desai, J. Rolston, L. Guo, and S. M. Potter, Front. Neuroeng. 2010, 3, 5.
- [37] E. Slavcheva, R. Vitushinsky, W. Mokwa, and U. Schnakenberg, *J. Electrochem. Soc.* **2004**, *151*, E226.
- [38] A. Hai, A. Dormann, J. Shappir, Y. Shlomo, C. Bartic, G. Borghs, J. P. M. Langedijk, and M. E. Spira, *J. R. Soc.*, *Interface* **2009**, *6*, 1153.
- [39] E. Vanhove, J. de Sanoit, P. Mailley, M.A. Pinault, F. Jomard, and P. Bergonzo, *Phys. Status Solidi A* **2009**, *206*, 9.
- [40] D. Hwang, T. Saito, and N. Fujimori, *Diamond Relat. Mater.* **2004**, *13*, 2207.
- [41] H. Choi, E. Gu, C. Liu, C. Griffin, J. Girkin, I. Watson, and M. Dawson, *J Vac Sci Technol B* **2005**, *23*, 130.
- [42] H. Uetsuka, T. Yamada, and S. Shikata, *Diamond Relat. Mater.* 2008, 17, 728.
- [43] C. Lee, H. Choi, E. Gu, M.D. Dawson, and H. Murphy, *Diamond Relat. Mater.* **2006**, *15*, 725.
- [44] M. Karlsson, K. Hjort, and F. Nikolajeff, *Opt. Lett.* **2001**, *26*, 1752.



- [45] J. Enlund, J. Isberg, M. Karlsson, F. Nikolajeff, J. Olsson, and D. Twitchen, *Carbon*, **2005**, *43*, 1839.
- [46] C. Lee, E. Gu, M. D. Dawsoon, I. Friel, and G. Scarsbrook, *Diamond Relat. Mater.* **2008**, *17*, 1292.
- [47] Y. Ando, Y. Nishibayashi, K. Kobashi, T. Hirao, and K. Oura, *Diamond Relat. Mater.* **2002**, *11*, 824.
- [48] T. Yamada, H. Yoshikawa, H. Uetsuka, S. Kumaragurubaran, N. Tokuda, and S. Shikata, *Diamond Relat. Mater.* **2007**, *16*, 996.
- [49] M. Hiscocks, C. Kaalund, F. Ladouceur, S. Huntington, B. Gibson, S. Trpkovski, D. Simpson, E. Ampen-Lassen, S. Prawer, and J. E. Butler, *Diamond Relat. Mater.* **2008**, *17*, 1831.

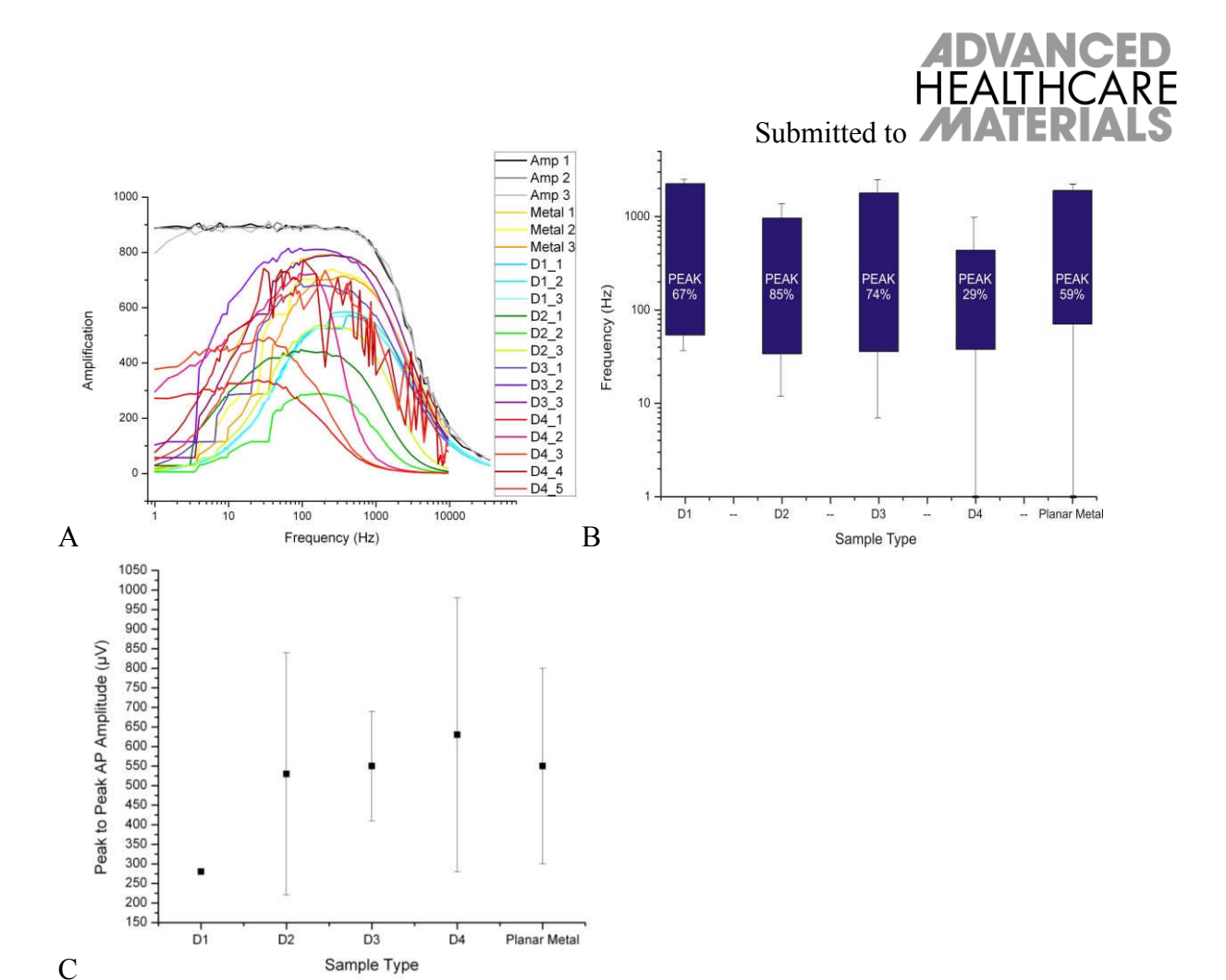


**Figure 1.** Electrical performance of MEAs. Amp = the amplifier system without any chip. Designs are described with electrode material/passivation material/bondpad material. D1 = BNCD/SU8/BNCD. D2 = BNCD/SU8/TiSi<sub>2</sub>. D3 = BNCD/ONO/TiSi<sub>2</sub>. D4 = BNCD/NCD/TiSi<sub>2</sub>. Planar Metal = Au/ONO/Au. All electrodes were 20 μm in diameter. A) Example amplification curves for the amplifier alone, Au MEAs, and the four different types of diamond electrode MEAs. B) Bandwidth of the BNCD MEAs is comparable to that of planar metal MEAs. The cutoff frequency is defined as  $1/\sqrt{2}$  of maximum signal amplitude achieved. Error bars are standard deviation of the cutoff frequency at each end of the band. N= 10, 9, 32, 55, 21, for D1-4 and metal respectively. Average peak performance is given for each band as a percent of the theoretical maximum. An ideal device would have 100% of the theoretical amplification over its bandwidth. In reality, this full amplification is rarely achieved. C) Despite low utilization of the amplifier capabilities, D4 devices exhibit good peak to peak values of recorded APs. N= 2, 5, 8, 7, 7 for D1-4 and Metal respectively. D1 does not have error bars because only 2 cultures were available.

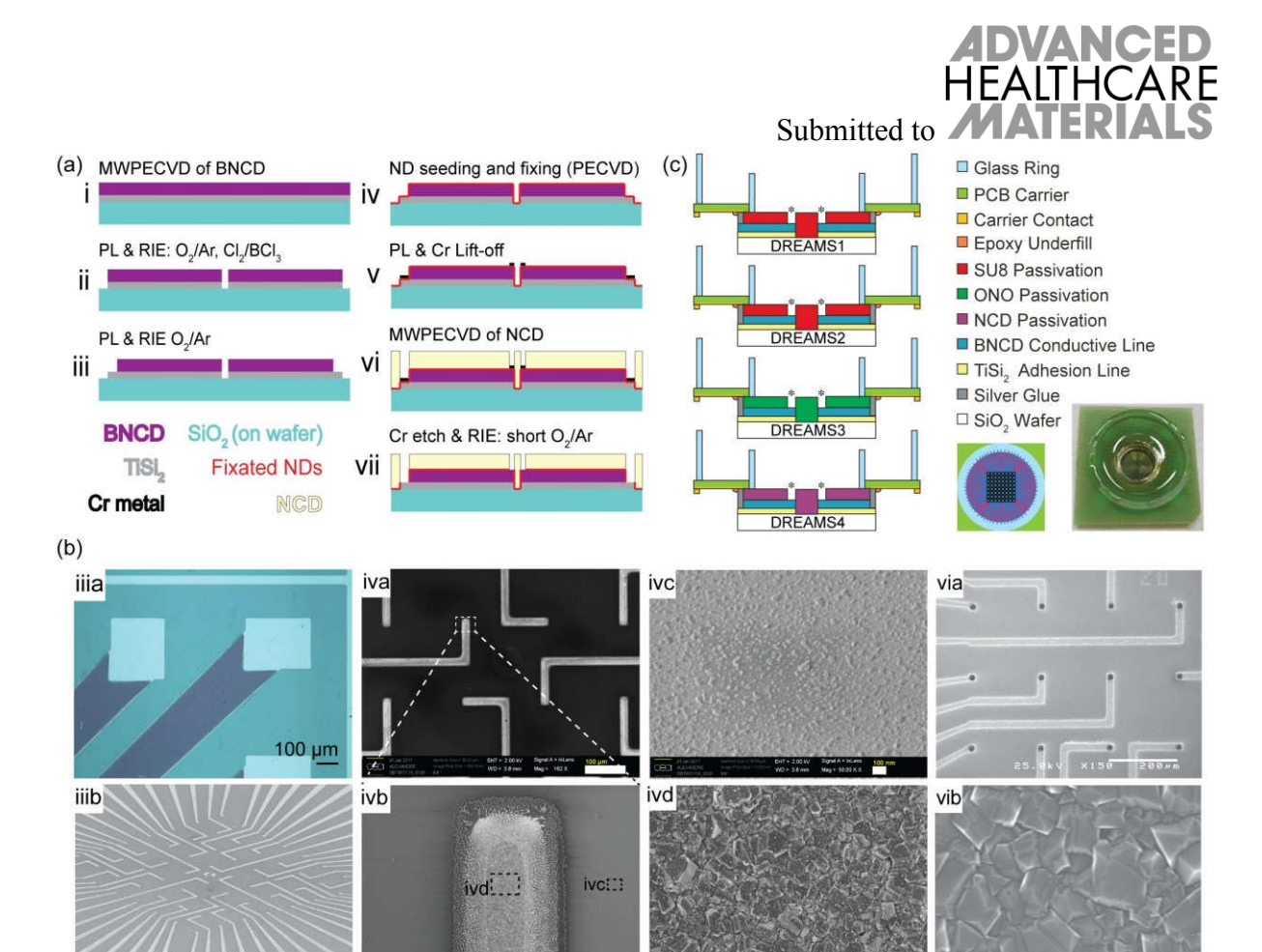


**Figure 2.** a)NCD-passivated BNCD/TiSi<sub>2</sub> MEA fabrication. PL: photolithography, MWPECVD: microwave plasma enhanced chemical vapour deposition, RIE: reactive ion etching. (b) Images of MEA corresponding to the process steps in (a). (iii.a) Optical image of exposed TiSi<sub>2</sub> bondpads and BNCD feedlines, scale bar 100 μm. (iii.b) Scanning Electron Microscope (SEM) image of MEA prior to passivation, scale bar 500 μm. (iv.a) SEM of MEA post-ND-seeding and MWPECVD fixation, scale bar 100 μm (iv.b) Enlarged image of an electrode, scale bar 2 μm. (iv.c) SEM image of NDs seeded on the the SiO<sub>2</sub> substrate, scale bar 100 nm and (iv.d) on the BNCD electrode, scale bar 200 μm, as labelled in (iv.b). (vi.a) MEA post-NCD MWPECVD growth, with electrodes covered by Cr caps, scale bar 200 μm. (vi.b) Magnification of NCD grown over the SiO<sub>2</sub> substrate, confirming the NCD nature of the material, scale bar 750 nm. (C) Schematic cut through of packaged chips with electrode openings marked (\*), including a schematic top view of the packaged BNCD electrode array and a photograph of the final MEA device.

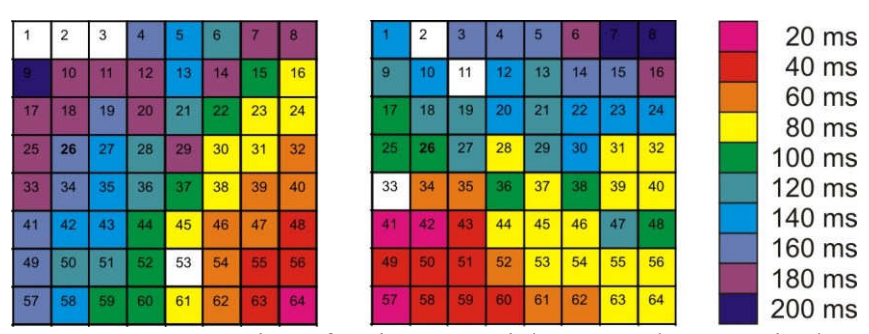


**Figure 3.** Propagation of action potentials across the MEA is shown by the time delay from the first spike to the time a spike is registered on each channel. Heat maps depict the spatial arrangement of the numbered measurement channels with 200  $\mu$ m pitch. On both planar gold MEAs passivated with ONO (left) and BNCD MEAs passivated with NCD (right) the action

potential takes similar time to cross the chip. On the gold MEA the pacemaker cell is to the bottom right of the array, while on the diamond chip the pacemaker is slightly higher and to the left of the array.

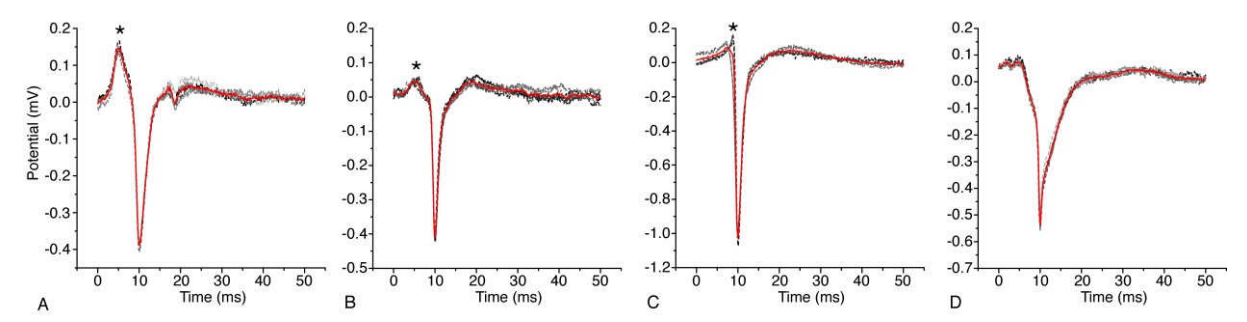


**Figure 4.** Individual APs (dashed gray) and average (solid red) recorded from a single channel aligned to the sodium peak. All BNCD electrode chips show a pre-spike indicating high seal resistance (\*). A) BNCD passivated with SU8, channel 10. B) BNCD passivated with ONO, channel 59. C) BNCD passivated with NCD and cleaned with plasma, channel 10. D) Planar gold passivated with ONO, channel 47. Note, the difference in scale, particularly for plots C and D.

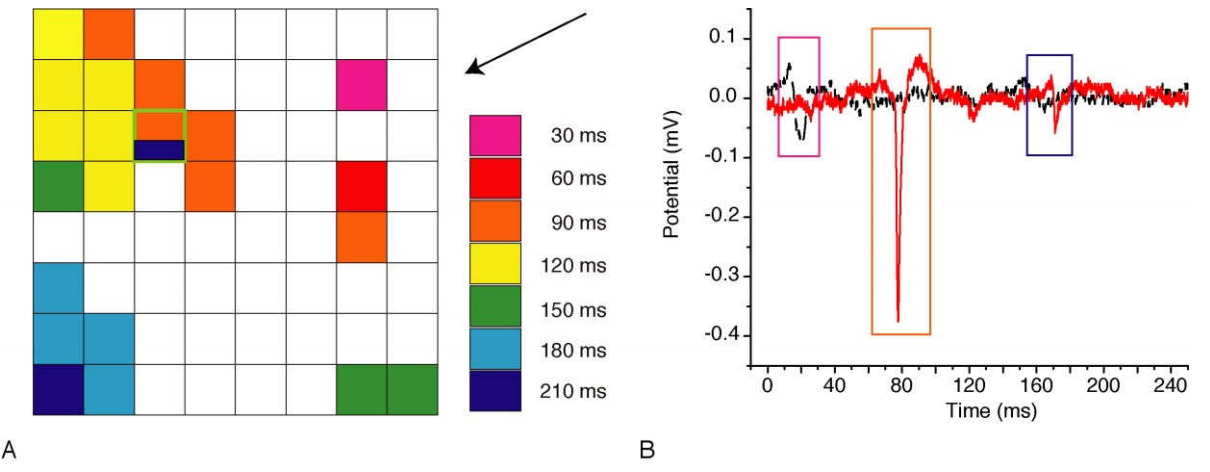


**Figure 5.** A) AP propagation is from upper right to lower left, as indicated by the arrow. A large spike arrives at electrode 19 (green outline) approximately 60 ms after the first spike at electrode 15 (pink fill). A second spike arrived later at Channel 19 via a passivation defect, as indicated in dark blue. Channel numbering is as in Figure 3. B) The potential recorded from Channel 19 (solid, red) and from Channel 15 (dashed, black). A larger spike is detected as the AP wave passes over electrode 19 than the spike detected from along the feedline that extends to the left (see Figure 2 (a)iiib for the feedline layout). Colored boxes correspond to the bins in A.

**Table 1.** The development of selective chemical etching of nanocrystalline diamond.

	Ar [sccm]	O <sub>2</sub> [sccm]	Pressure [mTorr]	CP [W]	PP [W]
Reported Ranges	8 <sup>44,45</sup> -25 <sup>46</sup>	7 <sup>44,45</sup> -90 <sup>40</sup>	2.5 <sup>44,45</sup> - 300 <sup>47</sup>	100 <sup>43,47</sup> - 1000 <sup>40-42,48</sup>	0 <sup>41,49,47</sup> - 300 <sup>43, 46</sup>
Recipe Developed	35	5	10	500	200



### The table of contents

Action potentials (white inset, horizontal scalebar 100 ms, vertical scalebar .1 mV) from cardiomyocyte-like HL-1 cells are detected by boron-doped nanocrystalline diamond electrodes with the diameter of single cells. Diamond passivated arrays are produced by a new non-reductive method. Confluent cells grow on the 64 electrode array in custom made culture structures (green), and the propagation of the action potential across the array can be mapped (color coded 10 ms bins, inset).

# Keyword nanocrystalline diamond

V. Maybeck, R. Edgington, A. Bongrain, J. Welch, E. Scorsone, P. Bergonzo, R.B. Jackman, and A. Offenhäusser\*

# Boron-doped nanocrystalline diamond micro-electrode arrays monitor cardiac action potentials

